Author response to the review of Young et al. “Rapid and accurate polarimetric radar measurements of ice crystal fabric orientation at the Western Antarctic Ice Sheet (WAIS) Divide deep ice core site” [Manuscript # tc-2020-264]

We would like to thank the two reviewers, Martin Rongen and Reinhard Drews, for their thorough, thoughtful and constructive reviews. Our initial response is available under Interactive Discussion, and we document the actual implementation of these changes below. Please find below the two reviewers’ comments (RC) in **bold**, each followed by the authors’ response (AC). Line, figure, and page numbers mentioned by the reviewers (within RC) refer to the original manuscript, and those mentioned by the co-authors (within AC) refer to the revised manuscript.

Review by Martin Rongen (30 October 2020)

General comments

RC1.1. The authors present a quad-polarimetric radar measurement at WAIS Divide. The dataset is interesting in its innovative nature as well as in the quality of the derived results. The method follows in direct succession to earlier works developed by Shuji Fujita and Tom Jordan among others. While previous measurements required a manual rotation of the antenna system in small steps in order to measure the azimuthal variation associated with the birefringence signature, the quad-polarimetric measurement allows for signal at arbitrary azimuths to be deduced from just four antenna orientations. The results are validated by comparison to ice core data.

The overall presentation is detailed and rigorous. Some improvements may be made by giving a clearer structure to the results and discussion sections (see later specific comments). As a non-expert on glaciological radar measurements, the theory and methods section was challenging but the provided references proofed to be very helpful. For the paper to stand on its own some more context/details may be added (see specific comments). Some more discussion may also be added to section 5.3 (Methods comparisons and limitations). It currently gives a fair comparison between radar and ice core / sonic measurements but is short on the specific limitations and assumptions involved in generating data for arbitrary azimuth angles using the quad-polarimetric data.

AC1.1. Thank you for your detailed review, and you as well as Reinhard Drews have correctly identified that we need to further discuss some method comparisons and limitations. We hope that we’ve addressed your concerns in the specific comments section below.

Specific comments

RC1.2. The readability of the results section would be greatly improved by structuring it in sub-sections, as is also done for the other sections. A possible structure could be:

- **4.1 Experimental results from WAIS (up to line 224)**
- **4.2 Modelling the observed data (lines 224-255)**
- **4.3 Fabric asymmetry estimation (lines 255 ff)**

AC1.2. Thank you for these suggestions. We have implemented these subsection titles with slight modifications:

- 4.1 Experimental results from WAIS Divide (L221)
- 4.2 Comparison between observed and modelled polarimetric signals (L259)
- 4.3 Estimation of azimuthal fabric asymmetry (L299)

RC1.3. The meaning of the pad factor mentioned in line 193 is unclear.

AC1.3. The pad factor refers to the amount of zero-padding applied to the time-domain signal relative to the total length of the original signal. We apply zero-padding to our data with a pad factor of 2, as recommended by Brennan et al. (2014). We have incorporated this description in L212-213: "Here, the pad factor represents the total length of the signal after zero-padding relative to the total length of the original signal." Note that this description has been moved to the end of Section 3.3 in response to RC2.17.

RC1.4. The details and reliability of the firn correction as introduced in line 198 are unclear. It is mentioned that this correction amplifies the estimated $E_2 - E_1$ values in the shallow ice and surprisingly large fabric asymmetries are then measured in that depth range. Thus the firn correction merits more attention (and maybe test without the correction) during the discussion (line 265 and 305) may be warranted.

AC1.4. We implement firn correction as suggested in the Appendix of Jordan et al. (2020a). Because the equation that drives this correction was derived from founding ice-penetrating radar principles (e.g. the ice-air volume fractions in the mixing relations of Looyenga 1965), we believe these corrections to be physically representative of firn anisotropy. Notwithstanding, we agree with your belief that the fabric asymmetries in firn are surprisingly large. We have therefore updated Figure 6 to include an inset that shows the effect of firn correction on resulting E_2 - E_1 values. We have added a sentence that justifies why we apply firn correction (L344-346): "As the applied firn correction is based upon established ice-air volume fractions in the mixing relations of Looyenga (1965), we believe these corrections to be physically representative of any fabric anisotropy within the firn layer." We then provide a physical explanation to why anisotropy is enhanced (L352-355): "Although comparative studies addressing the physical origins of fabric anisotropy do not exist for the firn layer, it is likely that the effects of prolonged firn densification on crystal rotation will induce some amount of azimuthal anisotropy within this layer (Burr et al. 2017)."

RC1.5. In line 196 it may be worth mentioning that the Jordan et al. (2019) prescription to evaluate $d\varphi_{hhvv}/dz$ is not actually based on the phase plot itself but on the real and imaginary components of the coherence as given in equation 7b.

AC1.5. We have clarified our methods with the inclusion of the following in L214-215: “We evaluated $d\phi_{hhvv}/dz$ using the real and imaginary components of c_{hhvv} (Eq. 7b) and estimated its respective error…”

RC1.6. The reasons for and consequences of switching from an FIR filter to the method described in l.197ff remain unclear.

AC1.6. We had used our method (a 2-D median filter + 2-D peak convolution) in a previous paper that processes 2-dimensional (x-z and y-z) imagery from a multistatic pRES array (Young et al. 2018). The reason for using this then was to remove high-frequency noise and speckle. We have also visually checked the filtered image to ensure that there are no remaining “rapid phase excursions due to a modulo 2π artefact” (Dall 2010). Our results are not sensitive to filtering within a wide range of parameters: we can validate our final results with equivalent ice core measurements, which allowed us to test several parameters as well as show that the choice of filter is not limited. Crucially, we increase our bulk depth resolution to 15 m compared with the 100 m used by Jordan et al. (2019), which shows the benefits of experimenting with different filters. Therefore, we are confident that the results of our method choices are comparable to and potentially exceed those of Jordan et al. (2019).

RC1.7. The anisotropy parameter β seems to be missing a unit (dB?) in the caption of Figure 3.

AC1.7. We had originally referred to β as the ratio between the (E-field) Fresnel reflection coefficient along the *y*-plane relative to the *x*-plane, and therefore β is supposed to be unitless. However, we think that expressing it in dB would relate better to birefringence. Therefore, we have redefined β to be the intensity ratio of anisotropic scattering and have rescaled the values to dB ($20 \log_{10}$). This is now in line with the majority of previous studies (e.g. Fujita et al. 2006, Jordan et al. 2019). This explanation is written explicitly in L142-146.

RC1.8. For depth greater than 1200 m (and to a lesser extent around 600 m) the derived $E_2 - E_1$ values become rather unstable. While this is commented on and partially reflected in larger error bars, a population of outliers with small fabric asymmetries as well as small error bars is a bit worrying. It may be beneficial to show a plot of the coherence magnitude. Given vanishing magnitudes, the phase becomes unconstrained leading to erratic $d\varphi_{hhvv}/dz$ values. In the deepest region the phase in Figure 2.e is more unstable as a function of depth than expected from the model calculation.

AC1.8. We agree with your suggestion to include $|c_{hhvv}|$. Your hypothesis that the outliers in Figure 6 (originally Figure 4) correspond to small $|c_{hhvv}|$ is correct: beyond 1300 m, values of $|c_{hhvv}|$ are generally <0.3, with increasing amounts of points removed with higher $|c_{hhvv}|$ thresholds. We have added a plot of $|c_{hhvv}|$ in Figure 4 (as well as Figures S1-10) as panel (d) to constrain the validity of these outliers, and have re-plotted Figure 6 with a $|c_{hhvv}|$ threshold of 0.3. We have included a description of the application of $|c_{hhvv}|$ in L312-319:

> “Even after filtering out E_2 - E_1 below a $|c_{hhvv}|$ threshold of 0.3 (green asterisks in Fig. 6), ApRES measurements beyond 1200 m show a marked increase in variability that, although centred around corresponding depth values in the WDC, varied between

0.04 to 0.42. We similarly observe a sevenfold jump increase in the associated standard deviation, ranging from values averaging 0.006 at depths of 200-1200 m to 0.04 within the depth range of 1200-1400 m. There exists a small cluster of four outliers with low values (E_2 - E_1 < 0.1) at depths between 1250 and 1350 m with anomalously low error bars, even after initial $|c_{hhvv}|$ filtering. Setting increasingly higher $|c_{hhvv}|$ thresholds to 0.4 and 0.5 removes these outliers as well as all calculated E_2 - E_1 values beyond 1250 and 1100 m respectively."

We have also added two sentences to Section 5.3 to suggest potential ways to overcome this limitation (L435-437): "High SNR does not always equate to high polarisation coherence (c_{hhvv}), and vice versa. It is, however, plausible that larger datasets that employ higher amounts of chirp-averaging may increase the SNR needed to extend beyond the current depth limitation of 1400 m."

RC1.9. The sentence "The birefringence of an individual crystal and its COF are related to the bulk ..." in line 97 reads a bit odd as a COF only applies to an ensemble of crystals. Maybe change to something like "the birefringence of individual crystals and their COF".

AC1.9. Your suggestion is good, and we have implemented this in the revised manuscript.

RC1.10. The term "depth step" in line 124 is a bit technical. Something like "depth where a reflection occurs" would be clearer to the reader.

AC1.10. We have replaced "... for each depth step and azimuthal orientation" with "... at each discrete scattering layer and azimuthal orientation", which is in line with the terminology used by Fujita et al. (2006) in their Section 2.2.

RC1.11. The meaning and relevance of the rotation matrix *R* as introduced in line 133 is unclear. To my understanding, it represents the rotation of the COF principle axis *of each traversed ice layer* with respect to a reference system defined by the antennas.

AC1.11. You are correct: the rotation matrix *R* is used in Equation 2 to reconstruct the theoretical signal components for each azimuthal shift θ, for which the component in question is either *T* (transmission between the antennas and the scattering layer) or Γ (reflection at the scattering layer). The use of *R* in essence replicates an azimuthal-rotational experiment (acquisitions made at each rotational increment of the antenna acquisition plane). The second half of the mentioned paragraph has been rewritten to now read (L137-140): "The rotation matrix *R*, with *R'* its transposition, is used in Equation 2 to reconstruct the theoretical signal components with respect to θ, for which the components are either *T* (transmission between the antennas and the scattering layer) or Γ (reflection at the scattering layer). *T*, Γ, and *R* are all 2x2 matrices and are each detailed respectively..."

Please also note that we have also redefined our rotation matrix to be [cos θ , -sin θ ; sin θ cos θ] (Eq. 4) as part of a larger restructuring of the definitions of *h* and *v* (see RC2.10).

RC1.12. It is mentioned that s_{hv} and s_{vh} should be identical given an ideal measurement. Has the difference between these two orientations been studied and the potential impact quantified?

AC1.12. In theory, $s_{hv} = s_{vh}$ which is well known according to the Lorentz reciprocity theorem. In practice, there will be small differences including (but not limited to): (i) differences in the beam pattern between the transmitting and receiving aerials, (ii) random clutter within the transmitted media; and (iii) human error in antenna positioning. This topic is well studied (e.g. there is a 100+ page book (Stumpf 2018) purely dedicated to antenna signal reciprocity!) but in general, the main differences between s_{hv} and s_{vh} are due to human error during data collection. In general, our data has minimal difference between s_{hv} and s_{vh}, although there is some additional variability seen at the near surface. This discrepancy may account for the mismatch between measured (Figure 4) and modelled co-polarised results (Figure 5) in the top ~200 m.

We have shown the additional variability in the near surface between s_{hv} and s_{vh} (note that this was incorrectly labelled as e in the previous draft) by modifying Figure 2 (originally Figure 2a, with the new figure shown below). We have added the description above regarding deviations from the Lorentz reciprocity theorem in L181-188. We have suggested this mismatch to be the link between the discrepancy between measured and modelled results in L294-296.

Additionally, sometimes $s_{hv} = -s_{vh}$ due to the 180° ambiguity in antenna position. This is true in our case, we state this anomaly in L187-188, and we explain further in AC2.3 and how this changes some of our figures and results.

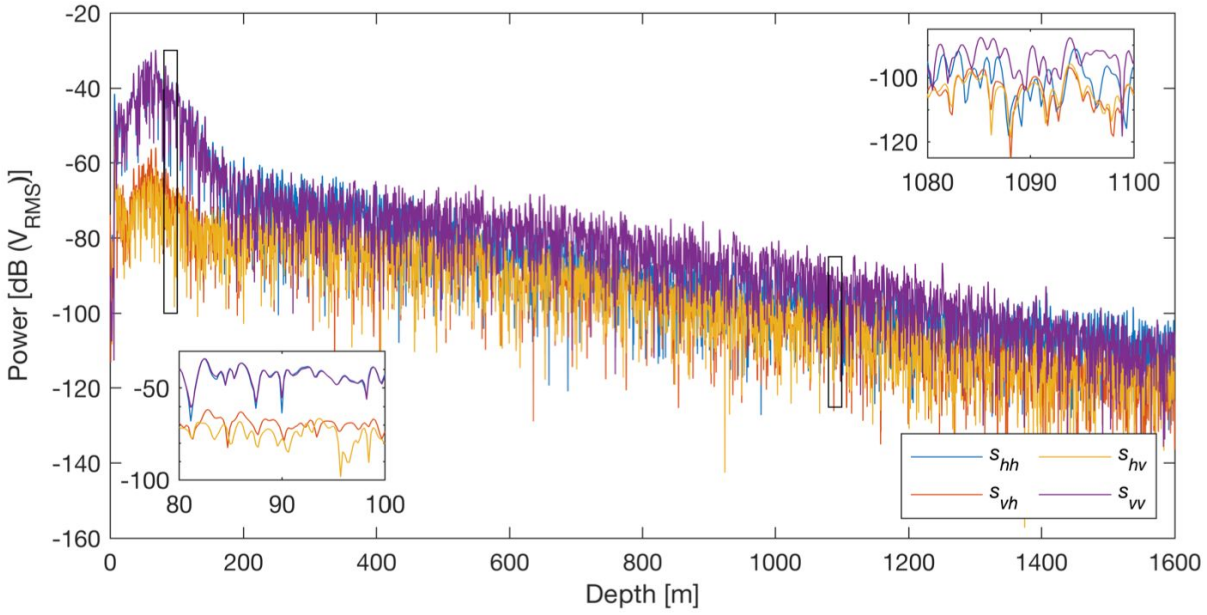

Figure. Mean (polarisation-averaged) power return for each antenna orientation. Insets show magnification of power returns at two different 20 m intervals (one shallow, one deep).

RC1.13. The COF orientation of each depth layer is resolved "by tracing the azimuthal minima in the cross-polarized power anomaly". While this may be a good

approximation for this measurement, I wonder if this technique is generally applicable in the presence of strongly varying COF orientations. Assuming, for example, a constant angle of 20° in the top 500 m and a constant angle of 60° below, my understanding is that the minimum in the cross-polarized power anomaly would only slowly migrate towards 60° below 500 m as the bulk propagation is initially still dominated by the conditions above. One essentially measures the average COF orientation up to the scattering depth. But there may be a misunderstanding on my part here. A comment would be appreciated.

AC1.13. In general, this method (as well as other published methods so far, e.g. Brisbourne et al. 2019, Jordan et al. 2020a) is accurate if the COF orientation is depth invariant. If the orientation undergoes an abrupt switch, such as the example that you propose above and below 500 m, the minima in power anomaly would similarly undergo an abrupt switch (e.g. at ~215 m in Figure 4 of Brisbourne et al. 2019). If this happens, the 90° ambiguity in the cross-polarised power anomaly plot would need to be resolved by either the co-polarised power anomaly or the co-polarised phase difference plots (see AC2.19). Additionally, there may also exist over or under-estimation of fabric asymmetry if the identified ice optic axis deviates from the true fabric orientation (e.g. Figure 4c of Jordan et al. 2020b).

We have summarised the above paragraph in Section 5.3 (L406-416):

> The cross-polarised power anomaly is generally a robust method of identifying the fabric orientation in slow-moving ice (Li et al. 2018). Here, we show that this method is reasonably accurate for depth-invariant eigenvectors (Fig. 4). In the case of a gradual rotation of the fabric orientation through depth, the cross-polarised power anomaly should undergo a similarly gradual rotation (Ershadi et al. 2021). This is also true in the case of an abrupt switch in COF, as evidenced at Korff Ice Rise (Brisbourne et al. 2019), where the cross-polarised power anomaly undergoes a similarly abrupt shift in azimuth. In elementary cases, the 90° ambiguity that exists in the cross-polarised power anomaly (Li et al. 2018) can potentially be resolved from the methods given in the previous paragraph. However, if the fabric orientation were to change rapidly with depth, using only the cross-polarised power anomaly to determine and distinguish between the two eigenvector orientations may produce erroneous results as demonstrated by Ershadi et al. (2021). In all cases, if the radar-derived fabric orientation is offset in azimuth from its true orientation, this mismatch will result in corresponding over- or under-estimation of azimuthal fabric asymmetry (Jordan et al. 2020b).

RC1.14. As noted in the general comments section 5.3 would benefit from a discussion of the specific limitations and assumptions involved in generating data for arbitrary azimuth angles using the quad-polarimetric data.

AC1.14. See AC2.4 for a discussion on the comparisons between quad-polarimetric and azimuthal rotational experiments.

RC1.15. Section 5.1 paragraph 2 (lines 281-288) seems better suited in section 4.1 (results, modeling), here a Figure similar to Figure 5 in the Fujita 2006 paper may also be illustrative, showing that birefringence results in nodes in the power anomalies while

anisotropic scattering results in a band structure, the spacing of which is a function of the scattering strength.

AC1.15. While a figure similar to Figure 5 of Fujita et al. (2006) may be useful, this specific figure has already been reproduced multiple times in subsequent papers (e.g. Figure 7 of Matsuoka et al. 2012, Figure 2 of Brisbourne et al. 2019) and we feel like there is already enough literature that describes the depth and azimuthal variability of the co-polarised nodes. Furthermore, we believe that Figure 5 (originally Figure 3) already serves the same purpose, in particular, a comparison between Figure 5a-c and 5d which shows the controls of anisotropic scattering (β) and birefringence ($\varepsilon(z)$, through E_2-E_1). Therefore, we do not reproduce Figure 5 of Fujita et al. (2006).

We have chosen to remove the second paragraph of Section 5.1, as (i) you have rightly pointed out that it would have been better suited in the Results section; and (ii) these statements are reminders of what has already been stated in the Results section as well as elsewhere, such as in the Introduction.

Technical comments

RC1.16. The link for the Mott, H. (2006) reference appears to be dead.

AC1.16. Thank you for pointing this out. We have fixed the link and ensured that it works.

RC1.17. In line 156, spectra so should be plural as are the amplitudes.

AC1.17. Corrected by changing “complex amplitudes” to the plural case (L172).

RC1.18. In the title of subsection 5.1 it would be more consistent to refer to "anisotropic scattering" instead of the more ambiguous "anisotropy"

AC1.18. We apologise for the ambiguity and have corrected the subsection title to now state “anisotropic scattering”.

Review by Reinhard Drews (19 November 2020)

Summary

RC2.1. In their paper ”Rapid and accurate polarimetric radar measurements of ice crystal fabric orientation at the Western Antarctic Ice Sheet (WAIS) Divide deep ice core site”, Young and co-authors present an ApRES radar dataset, which they use to infer the ice-fabric characteristics continuously to a depth of 1500 m. Main results include quantification of the horizontal ice anisotropy with a depth invariant ice-fabric orientation that is aligned with the directions of the principal strain rates. The inferences are validated with data from the WAIS ice core, and some conclusions are drawn about the ice-divide stability throughout the Holocene.

Overall, this paper is nicely written and the authors do a commendable job in guiding the reader through the methods and results. However, in places I find the paper unnecessarily superficial and I don't see novel aspects clearly. I also suspect (but I am not certain) that parts of the azimuthal reconstruction may be erroneous leading to wrong inferences in terms of the ice-fabric orientation. Below, I mention a number of major comments/questions how this can be improved. Applications of radar polarimetry are still rare, and I hope that the points raised below will help to improve the next version of this paper.

AC2.1. Thank you for your detailed review, and we appreciate your honesty in that you have disclosed your potential conflict of interest. We believe your review is unbiased and correctly identifies several areas will need to be addressed, specifically the three major comments (RC2.2 - 2.4). We have attempted to alleviate your concerns in our responses below. Ultimately, we hope that our paper can contribute to the radar polarimetry literature and advocate for radar as a robust tool to derive fabric strength and orientation estimates.

RC2.2. Clarify methodological advance

It is stated that this study "..extends previous qualitative analyses [...] to obtain quantitative measurements.." (l. 285). Can you highlight more clearly what those extensions were compared to previous studies? From what I can see so far, this study nicely applies previous developments to a single new site, but I struggle to see the extensions. The link between the polarimetric phase gradient and ice- fabric parameters is based on the cited papers Fujita et al., 2006 and Jordan et al., 2019. Arguably matching the angular distance of co-polarization nodes with a 2D optimisation is new (l.233), but at least the dependency of this distance as a function of anisotropic scattering is already approximated in Fujita 2006. Also advantages or pitfalls (e.g., in terms of uniqueness and uncertainties involved) of this approach are not discussed.

I suppose that this paper is the first to explicitly focus on synthesising quad-polarimetric measurements for ApRES, although the related methodology is known from radar polarimetry textbooks (e.g., the cited Mott, 2006). The inferences drawn from this method about the ”high angular” resolution are not credible as

currently presented (see comment below). Also the lack of rotational dataset at this site makes it hard to discuss advantages/disadvantages of both approaches. I suggest a dedicated section were improvements and distinct differences compared to previous studies are highlighted more explicitly.

AC2.2. In our opinion, this manuscript extends the literature (this being radar polarimetry for glaciological applications) through: (i) validation of co-polarised power anomaly and phase difference plots; (ii) publication of the quad-polarimetric reconstruction method; and (iii) direct validation of radar-derived measurements of ice fabric to that of ice cores at high depth resolution. We are fortunate that our results are simple to comprehend, and we believe that this, combined with the straightforward layout of the quad-polarimetric reconstruction method will help those who wish to apply radar polarimetric methods to glaciology. Due to the growing interest in radar polarimetry applications within the glaciological community as of late, we believe that our manuscript is not only valuable, but also timely for the above three reasons. In detail:

> (i) is shown through the direct comparison between measured (Figure 4) and modelled (Figure 5) results, where the birefringence in the latter was induced using fabric eigenvalues from thin-section analysis of ice cores. (The anisotropic reflection ratio is instead estimated through matching the locations of the co-polarised nodes, the four-quadrant patterns, and the *hhvv* phase with the measured results.) While we concede that the theory behind this comparison has previously been quantified in Fujita et al. (2006), they stop short of presenting modelled results complementary to their observations (in their case, fabric data from the Mizuho and Dome Fuji ice cores). Similarly, while fabric measurements from polarimetric radar measurements have been verified to ice core data by Jordan et al. (2019), they implement only the polarimetric coherence method (i.e. analysis of s_{hhvv}) and do not present any co- or cross-polarised datasets. On the other hand, Brisbourne et al. (2019) present co-polarised power anomaly and phase difference plots of radar measurements conducted at Korff Ice Rise but focus on the relative orientation of the antenna polarisation plane relative to the ice optic axis, and present only qualitative observations in terms of fabric strength. Our manuscript not only directly compares measured results to modelled plots, but also quantifies azimuthal fabric strength through the polarimetric coherence method and verifies results directly with ice core data. Therefore, our manuscript reconciles the methods of the above three studies.
>
> Regarding (ii), we felt a need to include the complete equations that show how the received signal (both power in Equation 4 and phase in Equation 5) can be reconstructed from quad-polarimetric measurements. You are correct in that these methods are established, and we do not attempt to take credit for them. However, these methods are often presented within dense literature specifically directed towards radar engineering applications and may be daunting for the majority of glaciologists (myself included!). Rather, we attempt to introduce them to the glaciological literature in an approachable format so that they are easily accessible for researchers wishing to conduct quad-polarimetric experiments.
>
> Regarding (iii), our results show that choosing a nominal depth-averaging window of 15 m (which is our nominal bulk-depth resolution) when applying the polarimetric

coherence method (Equation 6) produces estimates of azimuthal fabric asymmetry that closely match corresponding results from ice-core thin section data at similar intervals. While Jordan et al. (2019) also use the polarimetric coherence method to match fabric asymmetry estimates between radar and ice core measurements, also showing comparative results, they had chosen to use a conservative nominal depth interval (the bulk-depth resolution) of 100 m. Our study shows that this nominal depth interval can be reduced down to levels at or exceeding that of the vertical spacing of ice core thin sections, while still producing comparable results to ice core measurements. The ability to validate the processing parameters with ice core measurements gives confidence in both our methods and results.

As you may already know, there are multiple pitfalls in using the polarimetric coherence method, which are detailed in Jordan et al. (2019) and (2020a). We do not wish to regurgitate what has already been said, but we acknowledge that we have provided little caveats, which makes it seem like we are "overselling" our results. We have separated what was Section 5.3 (Method comparisons and limitations) into two sections: Section 5.3 (Radar polarimetric methods to determine fabric strength and orientation) and Section 5.4 (Broader comparisons of geophysical methods to infer ice fabric properties).

There are 5 paragraphs comprising Section 5.3. The first paragraph highlights the strengths of this study with reference to its similarities and differences from previous studies of power anomaly and polarimetric coherence. The second paragraph describes how to distinguish between the two horizontal eigenvector orientations (see AC2.16). The third paragraph critiques the use of the cross-polarised power anomaly to identify the ice optic axis (see AC1.13). The fourth paragraph presents a discussion between azimuthal rotation methods and quad-polarimetric measurements (see AC2.4). The fifth paragraph discusses the signal-to-noise ratio, the hhvv coherence, and how this may be overcome (see AC1.12).

RC2.3. Coincidental symmetry at $\theta = 90°$?

In Figs. 2b-e one principal axis of the ice-fabric appears at the local azimuthal angle $\theta = 90°$ (i.e., all panels have a reflectional or rotational symmetry around the $\theta = 90°$ axis). This means that during measurements antennas were coincidentally placed parallel (*hh*) and perpendicular (*vv*) to the (at the time) unknown ice-fabric orientation. It is possible that the operators in the field made a conscious decision here because $\theta = 90°$ aligns with the strain rate (not the ice-flow) direction. However, given uncertainties involved in determining the direction of maximum strain rate and the antenna orientation, the $\theta = 90°$ symmetry almost seems too much of a coincidence. Based on our own experience with analysing quad-polarimetric data, we suggest that the authors double-check that indeed $s_{hv} = s_{vh}$. We found occasionally that $s_{hv} = -s_{vh}$ without satisfying explanation as to why this can be the case (e.g., inconsistencies in labelling and naming of antenna orientations in the field?). However, if it is the case, then reconstruction of the ApRES signal using eq. (4) forces a symmetry axis at $\theta = 90°$ exemplified below for the s_{hh} component:

$$S_{11} = s_{hh}(\theta) = \underbrace{\underbrace{s_{hh}\cos^2\theta + s_{vv}\sin^2\theta}_{\text{symmetric at } \theta=90^\circ} + \underbrace{(s_{vh}+s_{hv})\sin\theta\cos\theta}_{\text{anti-symmetric at } \theta=90^\circ}}_{\text{in general no symmetry axis at } \theta=90^\circ \text{ unless } s_{hv}=-s_{vh}}$$

The graphic below illustrates how this would be reflected in a full azimuthal reconstruction where the principal axis around *θ* = 35, 125° in the top plot are erroneously mapped to *θ* = 90, 180°. Without a co-polarized, rotational dataset this will occur unnoticed.

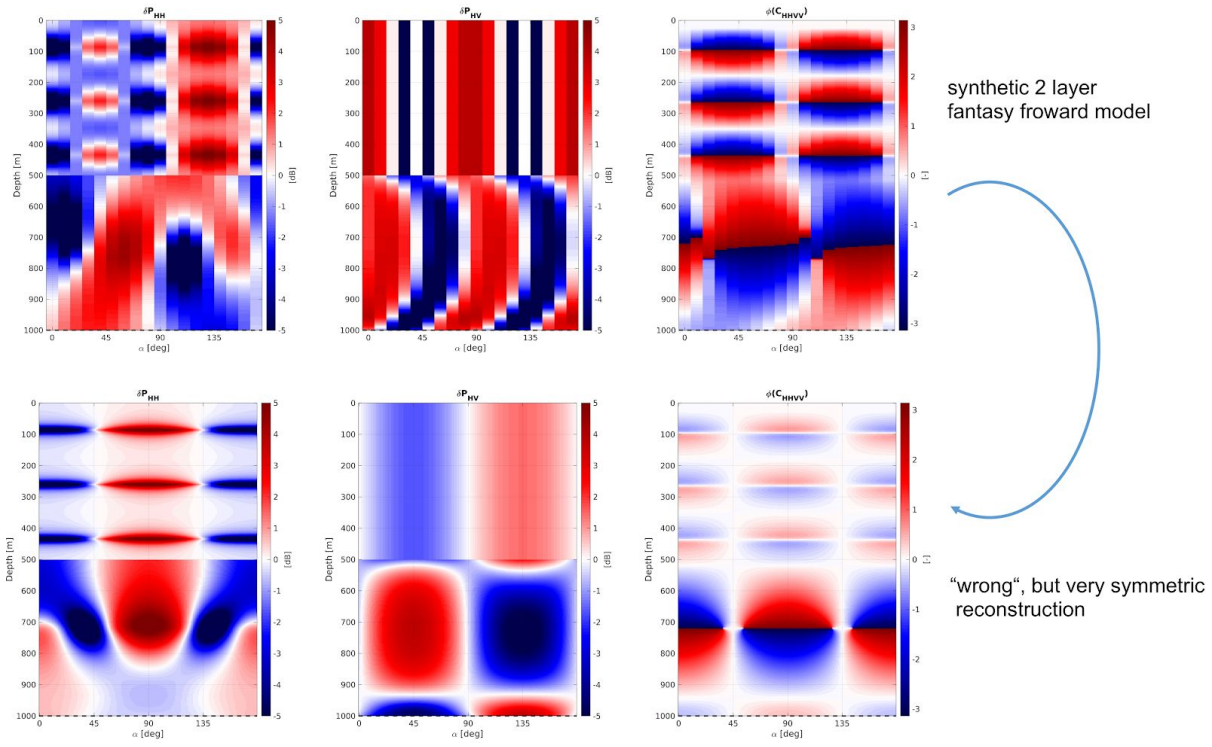

Maybe it will be helpful to investigate this further. Alternatively, state explicitly how the *hh* and *vv* directions were defined in the field, and why it makes sense that those axis align almost perfectly with the principal directions of the ice-fabric.

AC2.3. Your suspicions in the exact alignment of the antenna polarimetry plane in Fig. 2 with the strain axes is warranted. In our initial manuscript submission, we show the results from one ApRES site, but we did not mention in our manuscript that we had also obtained ApRES measurements from nine other sites along a ~6 km-long transect. We have included the transect in the updated Figure 2. We now include results from all 10 sites in Figures S1-S10 and results from all sites are consistent with each other. The results displayed in Fig. 4 (originally Fig. 2) represents Site I, and is the 9th of 10 total sites in terms of their relative position along the transect. The antenna axis (i.e. the plane that runs between the transmitting and receiving antenna) is orthogonal to the transect line, and we have clarified this in the text as well as in Figure 1 (see AC2.10). This is opposite to the assignments we had used in the original TCD manuscript draft (i.e. *h* is now *v* and *v* is now *h*), and therefore all plots had shifted by 90°.

Upon re-inspection of our code, we noticed a rounding error when importing the Northing and Easting coordinates that resulted in the antenna polarisation plane to be aligned exactly with the direction of maximum compression. In reality, the antenna polarisation plane is actually +7° (where positive numbers represent counterclockwise directions) from the strain compressive axis (rounded to the nearest degree). The orientations of velocities, strain axes, antenna axes, and eigenvectors have all been double-checked and should now all be consistent with each other.

Using data collected at Site I (the data used to produce Figure 2 in the initial TCD manuscript), we present in Figure AC1 2 sets of plots of co- and cross-polarised power anomaly and phase difference. Set 1 (panels a) assumes that $s_{hv} = s_{vh}$, and set 2 (panels b) assumes $s_{hv} = -s_{vh}$. In these figures, the mean and standard deviation of the E_1 (green) and E_2 (yellow) eigenvectors for panels (a) were calculated to be 90.3° ± 3.98° and 1.8° ± 3.81° respectively, and for panels (b), -90.6° ± 6.06° and -2.7° ± 5.99° respectively, using the same methods described in the TCD manuscript. Figure (AC1) shows that the eigenvectors were oriented at or very close to 0 and 90° irregardless of signage. Note that the x-axes are shifted 90° due to our re-assignment of *h* and *v* with respect to the E-field (see AC2.10).

However, because the two results give approximately the same results, we are not able to determine whether or not panels (a) or (b) shows the correct polarimetric patterns from Figure (AC1) alone. We then run the same investigation on the other 9 sites and show the output plots from one of these sites (Site D) in Figure (AC2). We regard the results shown in Figure (AC2) to have higher variability between results produced using each of the two assumptions in turn, but overall representative of all sites. With the additional consideration of Figure (AC2), we can say that all sites are centred about 0° regardless of the signage of s_{hv} and s_{vh}, but the assumption that $s_{hv} = -s_{vh}$ produces realistic variations between the plots whereas $s_{hv} = s_{vh}$ essentially produces replicates of the co-polarised power anomaly regardless of the site, which may or may not match its cross-polarised power anomaly. For the example site (Site D) shown in Figure (AC2), the plots produce an E_1 and E_2 eigenvector orientation 98.9° ± 4.71° and -7.5° ± 4.68° despite having a co-polarised power anomaly plot centred around 0° under the first assumption ($s_{hv} = s_{vh}$, Figure AC2a), while the co-polarised and cross-polarised power anomaly plots are consistent with each other with the eigenvectors at 101.6° ± 5.96° and 7.4° ± 4.43° under the second assumption ($s_{hv} = -s_{vh}$, Figure AC2b). We assume that the deviation of the principal axis from exactly 90° in both assumptions are primarily the result of human errors in antenna positioning, as well as lateral migration of the ice optic axis across distance.

Assuming that the four orthogonal combinations of antenna orientations were conducted in the same way for all 10 sites (which, to the best of our knowledge, is true), the results from Figure (AC1) and Figure (AC2) show that (i) the positions of [*h* | *v*] and [*v* | *h*] that we used in the field (Figure 1a) correspond to the second assumption that $s_{hv} = -s_{vh}$; (ii) the use of the cross-polarised power anomaly in determining the principal axis is valid regardless of whether the first or second assumption is used; and (iii) the lateral eigenvectors for Site I about 90° and 0°, and aligned with the strain axes, is valid as well as being fortuitous.

Given the new knowledge gleaned from this investigation, we have:

a. Re-processed our datasets using the assumption that $s_{hv} = -s_{vh}$, with an explicit mention in the methods (L187-188);

b. Updated our estimate of relative orientation of the E_1 and E_2 eigenvectors to 91° and -3° from the results of the re-processing;
c. Provided equivalent plots of Figure 4 for all 10 sites along the transect in the Supplementary Information as Figures S1-S10, with collated results in Table S1. The 10 sites show consistency across the entire transect;
d. Updated the modelled anisotropic scattering parameter and therefore updated Figure 5 to match the re-processed Figure 4.

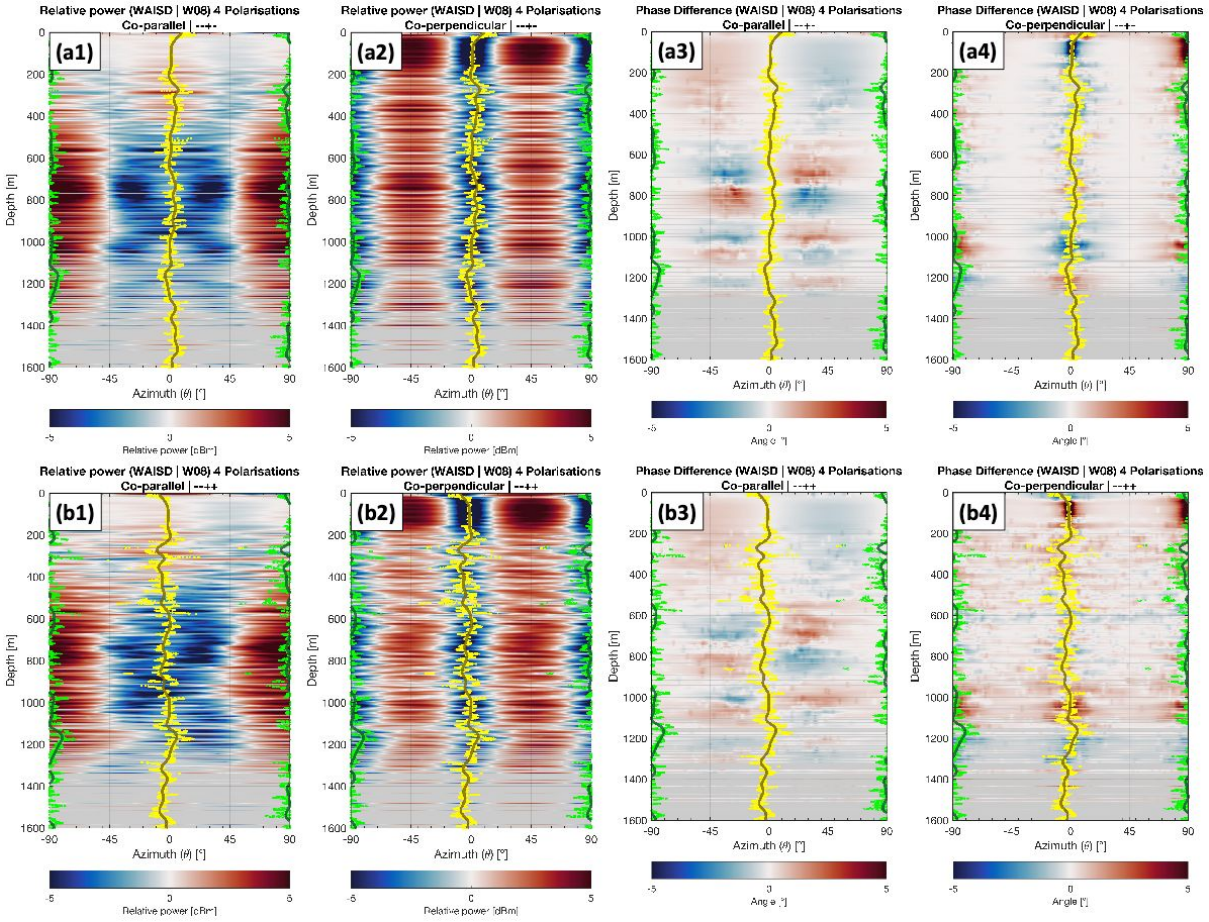

Figure AC1. ApRES polarimetric power anomaly and phase difference measured at Site I, WAIS Divide. (Note that this is labelled as W08 in these plots as these are our internal numbering system) The top row of panels (a) were produced assuming $s_{hv} = s_{vh}$, and the bottom row of panels (b) assume $s_{hv} = -s_{vh}$. Columns (1) show co-polarised power anomaly, columns (2) cross-polarised power anomaly, columns (3) co-polarised phase difference, and columns (4) cross-polarised phase difference. Bright green dots represent azimuthal minima at each range bin, and the dark green line is the best estimate of the symmetry axis calculated using a Gaussian-weighted moving average of the azimuthal minima. Depths with insufficient SNR are greyed out.

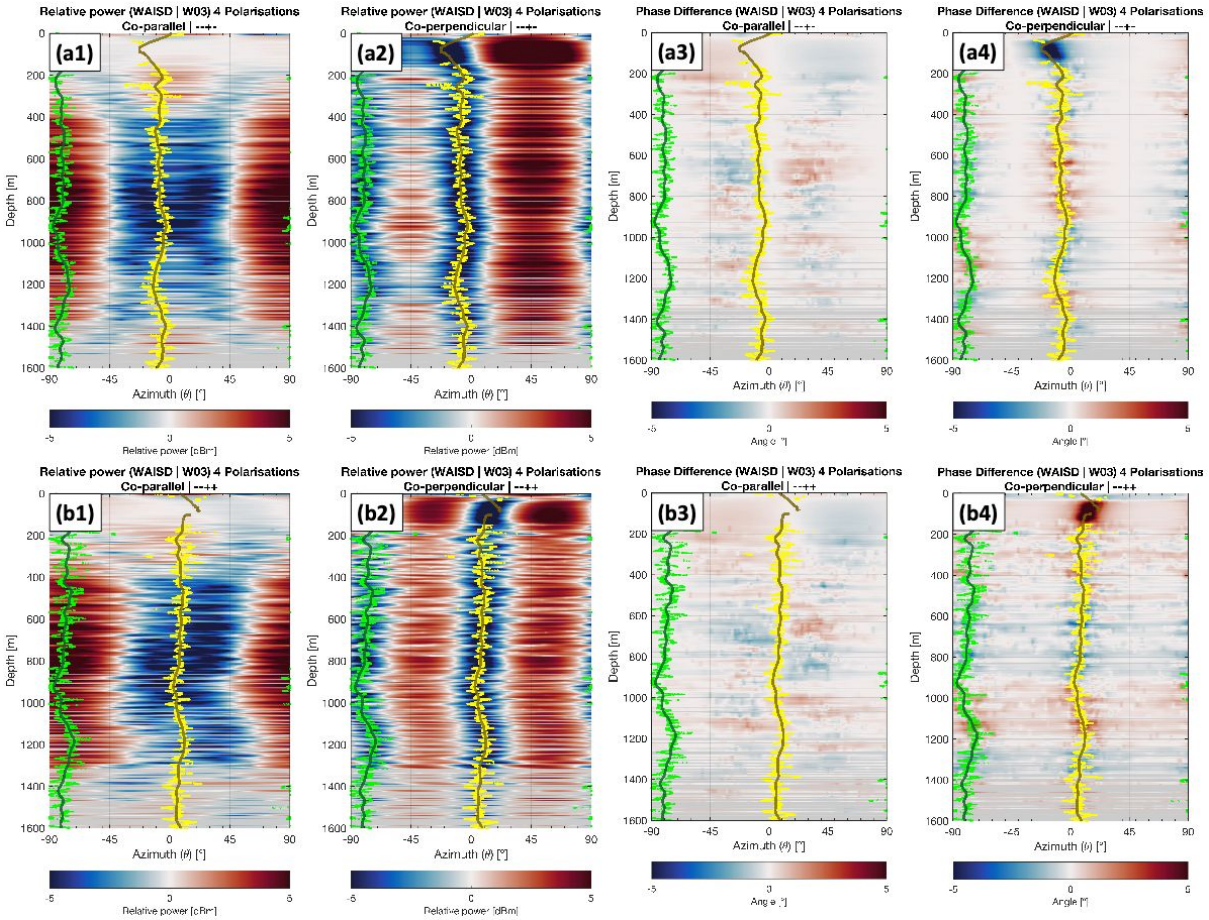

Figure AC2. ApRES polarimetric power anomaly and phase difference measured at Site D, WAIS Divide. Legends are identical with those for Figure AC1. (Note that this is labelled as W03 in these plots as these are our internal numbering system)

RC2.4. Terminology linked to azimuthal resolution

In numerous instances (e.g., l.7, l39, l49..) the authors advertise that synthesizing the azimuthal response from quad-polarimetric data (eq. 4) results in improved angular resolution compared to rotational setups. I disagree with that. The chosen azimuthal spacing of 1° (l. 397) is completely arbitrary and any value works with eq. 4. I agree that advantages and disadvantages of quad- polarimetric vs. rotational measurements should be discussed, but choosing an arbitrary gridding for θ is not enough in this regard. Also, no rotational dataset is presented so that the claims about the superiority of quad-polarimetric measurements are not rigorously substantiated (apart from the obvious fact that they are much quicker to obtain).

AC2.4. Unfortunately we did not conduct azimuthal rotational measurements at WAIS Divide and so we are unable to make a full and direct comparison between quad-polarimetric and rotational measurements specifically with regards to our own datasets at WAIS Divide. However, comparisons between the two field methods were made when analysing ApRES data from Brisbourne et al. (2019) of which we found minimal difference in the results generated from the two methods.

That being said, Matsuoka et al. (2012) conducted an azimuthal rotational survey close to (~5 km from) our study site of which the results are shown in their Figure 3, Panel SW-24. Although they had used radar systems with different frequencies from ours (60 and 179 MHz as opposed to 300 MHz for ApRES), we can see that, at least to 1400 m, our estimate of the fabric orientation matches their results.

We acknowledge that we cannot fully claim the superiority of one measurement method over the other without conducting both at the same study site. We therefore add a paragraph in Section 5.3 that compares the two methods (azimuthal rotational measurements v. quad-polarimetric measurements) and cites recent papers (notably that of Ershadi et al., 2021) in addition to comparing our results with that of Matsuoka et al. (2012) to state that there should be no structural differences between the outputs of both methods (L417-429):

> Because we did not conduct azimuthal rotational measurements at our study sites, we are unable to make a full and direct comparison between quad-polarimetric and rotational measurements in terms of their output results, and therefore are unable to advocate for one method over the other. However, a visual comparison between our results and those obtained at Site S-W24 of Matsuoka et al. (2012) show similar polarimetric power anomalies in the upper 1400 m of ice, which give us confidence in our results. Separately, comparative analyses of results obtained using both types of measurements at Korff Ice Rise (C. Martin, *unpublished data*) as well as at EPICA Dronning Maud Land (Ershadi et al., 2021) reveal no structural differences between datasets. This comparative similarity may not hold in areas with more dynamic and/or complex flow, where the E_3 eigenvector is not vertically-aligned, and requires further investigation. While our estimation of the E_1 and E_2 eigenvector orientations in our measurements is to the nearest 1°, this precision reflects the angular bin size used to azimuthally reconstruct the received signal from quad-polarised data in this study, and is not synonymous with angular resolution, which instead is largely dependent on human errors in positioning the antennas for each acquisition (here assumed to be

±8°). However, under the assumption that the two acquisition methods do produce physically equivalent datasets, then a quad-polarimetric reconstruction allows for a comparatively higher precision in the identification of the two eigenvector orientations.

Minor remarks

RC2.5. Abstract should state limitation that the methodology only works if one of the c-axis is pointing upwards.

AC2.5. You make a fair point. We have explicitly mentioned this limitation in L3-4: "... at radar frequencies, with the assumption that one of the crystallographic axes is aligned in the vertical direction."

RC2.6. l 57: Eq. 4 reconstructs the azimuthal response, but this is something different than resolving it. See comments above.

AC2.6. See AC2.4 for a detailed response. For this specific reference, we have removed this claim in the sentence which now reads (L58-59): "This quadrature- (quad-) polarised setup significantly reduces the field time required to obtain each set of acquisitions."

RC2.7. l 63: Specify what resolution you refer to. ApRES surely has lower potential for vertical resolution than ice-core data.

AC2.7. ApRES certainly has lower resolution potential than ice-core data and we apologise for not being specific. The issue with defining the vertical resolution of ice cores is due to allocation of core sections to different scientific goals (at least, to the best of my knowledge), so while the depth resolution of ice cores in terms of fabric eigenvalue estimates can potentially be down to the centimeter scale, in practice the thin sections used to estimate eigenvalues are taken at larger intervals (~50-100m for the WAIS Divide ice core). The depth resolution of ApRES refers to the bulk-averaged fabric of the local depth window (15 m in our case). We remove our use of "resolution" and instead use terms like "bulk-averaged depth resolution" and "depth interval" for the vertical resolution of ApRES measurements of ice fabric. "Bulk-averaged depth resolution" follows the terminology of Jordan et al. (2019). For example, the lines referenced in this comment now state (L62-64): "...at a nominal bulk-averaged resolution of 15 m. We show that, using this setup and method, our estimates of fabric asymmetry are comparable to that from ice core thin sections taken at similar depth intervals. From our results, we explicitly determine…"

RC2.8. l 65: Specify what the angular resolution is. It cannot be the 1° . I would also prefer more modest wording for "unambiguously". Defining the direction of the ApRES antennas alone is already error-inflicted and there is no rigorous statement in this paper on how this was done.

AC2.8. We have replaced "unambiguously identify" with "explicitly determine". Because there is ambiguity in the attribution of angular resolution to either the model azimuthal bin size (1°) or the accuracy of orienting the antennas, we have removed "...to high angular resolution"

from this sentence. We state how we define the antenna orientation in L162-163 (see AC2.10 for a full description).

RC2.9. Overall nice structure of the introduction. This works for me.

AC2.9. Thanks for the compliment!

RC2.10. Fig. 1a include orientation of the E-field vector. Statement that antennas are oriented parallel to the divide is conflicting with inference that principal axis is at θ = 90° (which is parallel to flow, which is oblique to the divide according to Fig 1b). See major comment 2.

AC2.10. There is probably a confusion that originates from the assignment of *v* and *h*. In the original TCD submission, we followed the conventions of Brisbourne et al. (2019) and defined *v* to be parallel to the antenna E-plane (which *h* is perpendicular to the E-plane). In this revised draft, we opt for consistency among the recent wave of radar polarimetry manuscripts-in-submission, and switch to using the convention presented in Figure 2 of Ershadi et al. (2021), where alignment nomenclature corresponds to the E-field vector. Therefore, in our revised draft, *hh* now becomes *vv*, *hv* becomes *vh*, etc. This has been updated in Figure 1 (in which panels (a) and (b) are now in separate figures) which also includes the E-field vector. All plots are therefore shifted so that the x-axis is now [-90° +90°], and θ therefore now represents the angle from the antenna plane, which is orthogonal to our transect direction and ~parallel to WAIS Divide. The angle stated here (250°) is correct but the orientations of the velocity vectors and Divide orientation are not, and this has been updated in Section 2 and 3 to have all orientations be consistent.

We also explicitly write that the nomenclature of *h* and *v* vary between manuscripts (L164-167): “The nomenclature attached to the *h* and *v* alignments are indicative of the electric field (Fig. 1) and are consistent with those used in polarimetric ApRES studies of ice fabric (Jordan et al., 2019, 2020b, Ershadi et al., 2021) with the exception of Brisbourne et al. (2019), which reverses the two assignments (i.e. *h* in our study corresponds to *v* in their study, and *v* in our study study corresponds to *h* in their study).” This discrepancy took us some time and frustration to realise, and we hope that this statement can aid in preventing future confusion.

Because we depart from the *h* and *v* nomenclature of Brisbourne et al. (2019), we also forego the use of “symmetry axis”. We instead define the axes identified by the cross-polarised power anomaly as the E_1 and E_2 eigenvector orientations, and distinguish between the two using the sign of the *hhvv* phase derivative following Jordan et al. (2019).

RC2.11. l 114 not only ice-dynamics but also ice properties induced through climate variations imprint on the ice-fabric evolution. I am not sure the principal ice-fabric axis always line up with today’s strain rate regime as suggested here.

AC2.11. We have included mention of climate effects with the addition of the following sentence (L114-115): “In addition, fabric strength and orientation are also influenced to some extent by perturbations in climate (Kennedy et al. 2013).” We have reduced the certainty of the sentence regarding how the fabric axis lines up with the strain rate regime, and moved

this to be specific regarding the vertical girdle (L120-122): “In the case of a vertical girdle fabric, the *c*-axes are oriented in a girdle that is planar to the E_2 and E_3 eigenvectors, with the E_1 eigenvector indicative of the orientation of lateral flow extension at its corresponding age-depth (Brisbourne et al. 2019; Matsuoka et al. 2012).”

RC2.12. l 127 the terminology ”anisotropy” for *β* has confused me. You also need ”anisotropy” for birefringence. Why not call it the ”anisotropic reflection ratio” or something like that? ”boundary reflection” is more appropriate than ”boundary scattering” (the latter suggests some diffuse scattering which is not accounted for in this context. However, this may be a matter of taste.)

AC2.12. We have redefined *β* to be the *intensity ratio parameter for anisotropic scattering*, in line with the majority of the previous radar polarimetric studies (e.g. Fujita et al. 2006, Drews et al. 2012). See AC1.7 for a full explanation.

RC2.13. l 137 remove abbreviation SISO. It is not used later on.

AC2.13. Removed. We have similarly removed the abbreviation “MIMO” in the same paragraph for the same reason.

RC2.14. l 150 include uncertainties for this angle here and elsewhere.

AC2.14. See AC2.18.

RC2.15. l 169 double-check that $s_{vh} = s_{hv}$ (see comment above).

AC2.15. We address this comment in AC2.3.

RC2.16. I understand how this azimuthal phase difference is calculated, but I don’t understand what the additional value is. What inferences are drawn from the co-polarised phase difference that cannot be drawn from the hhvv phase angle?

AC2.16. The four-quadrant patterns in the co-polarised (*hh*) phase difference plots are coincident with the location of the nodes in the co-polarised power anomaly plots (Brisbourne et al. 2019). The location of these nodes and four-quadrant patterns then constrains the 90° ambiguity in the cross-polarised (*hv*) power anomaly (see AC2.19). We find it to be more clear to locate the nodes and check the fabric orientation using a combination of investigating the co-polarised nodes and four-quadrant patterns (as in Brisbourne et al. 2019) than in the *hhvv* phase angle plot. Having the co-polarised power anomaly and phase difference plot may be useful in case of an abrupt shift in fabric orientation (again, as evidenced in Brisbourne et al. 2019).

Because we choose to define *h* and *v* differently to Brisbourne et al. (2019), the four-quadrant patterns are now centered on the E_2 axis (they were centered on the E_1 axis in Brisbourne et al. 2019). However, we choose to still include this in the manuscript as it allows readers to see the relationship between power-based, phase-based, and (*hhvv*) coherence-based methods and connects past studies with recent, quantitative studies. We

also provide this explanation as an additional way to distinguish between the two eigenvectors (L401-405):

> However, if anisotropic scattering is present, the azimuthal location of the four-quadrant patterns in the co-polarised phase difference is also an effective way to discriminate between the two eigenvectors (Brisbourne et al. 2019). Here, the four-quadrant patterns are centred around the E_2 eigenvector (Fig. 4c, Fig. 5c). Although the results of Brisbourne et al. (2019) observe the patterns to instead be centred around the E_1 eigenvector, we can reconcile this discrepancy due to opposite assignments of *h* and *v* antenna alignments used between the two studies.

RC2.17. l 193 This first paragraph is more methods to me than results.

We have moved the sentences “A pad factor of 2… with the same moving matrix dimensions.” to the end of Section 3.3, with slight alterations to the phrasing to account for its new placement. We have also added an explanation of the “pad factor” term within these sentences to address RC1.3.

RC2.18. As stated above the 90° are suspicious. Also, what are the ±7° based on? I would think that errors in antenna positioning are larger.

AC2.18. (Note that our definitions of *h* and *v* are switched and all measurements are shifted by 90°, see AC2.10) In AC2.3, we note that the E_1 eigenvector is more or less symmetric about 0°. The ±6° (originally 7°) is the standard deviation of the calculated eigenvector orientations from the cross-polarised power anomaly at each depth bin (azimuthal minima, bright dots for the E_1 (green) and E_2 (yellow) eigenvectors in Figure 4). These errors are unrelated to antenna positioning. We have adopted Brisbourne et al. (2019)’s nominal assignment of ±8°as the human error associated with antenna positioning (L163-164). We have stated the independence of the two errors in L250-251.

RC2.19. l 213 Typo? This ambiguity cannot be resolved in the *hh* power anomaly shown in Fig 2b. You need to use the polarity of the phase gradient.

AC2.19. On the contrary: if anisotropic scattering is present in the imaged ice, the 90° ambiguity in the cross-polarised (*hv*) power anomaly can be resolved by determining either (i) the azimuthal minima of the co-polarised (*hh*) power anomaly plot, or (ii) the azimuth of the centre of the four-quadrant patterns in the co-polarised phase difference plots, as stated in Section 5.1 of Brisbourne et al. (2019). If co-polarised nodes are weak due to strong anisotropic scattering, the sign reversals in the four-quadrant patterns remain diagnostic. On the other hand, if there is no anisotropic scattering present, then both the co-polarised power anomaly and phase difference plots will present 90° ambiguity as shown in Figure 2a of Brisbourne et al. (2019).

This being said, we rely on the polarity of the phase gradient in resolving the E_1 and E_2 eigenvectors in the revised draft (see AC2.16). We have modified this section to now reflect our updated analysis (L241-247):

By tracing the azimuthal minima in the cross-polarised power anomaly profiles through depth (Fig. 4c), we can identify the orientations of the E_1 and E_2 eigenvectors (Li et al., 2018). However, because there exists a 90° ambiguity in the cross-polarised power anomaly profiles, we rely on the sign of the gradient of the *hhvv* phase angle (Fig. 4e) to distinguish between the two eigenvectors. Because the the E_1 and E_2 eigenvectors align with the directions of the smallest and largest dielectric permittivities respectively, the location of the azimuthal minima resulting in a negative Φ_{hhvv} gradient through depth indicates the direction of the E_1 eigenvector, and the azimuthal minima resulting in a positive Φ_{hhvv} gradient indicates the direction of the E_2 eigenvector (Jordan et al., 2019).

RC2.20. l 221 at least estimate these "human" errors

AC2.20. See AC2.18.

RC2.21. why is the "anisotropy" an integer value?

AC2.21. This comment is a duplicate of RC1.7, please see our response there.

RC2.22. l 237 I think I missed something here: Aren't those node pairs simply depths where the phase shift between ordinary and extraordinary wave is odd integer multiple of π ? Clearly they will have a correspondence in the azimuthal phase difference (which is directly related to the phase angle). I don't understand the deeper physical implication of this 'four quadrant pattern yet.

AC2.22. See AC2.16 for further discussion on the relevance of the co-polarised phase difference.

RC2.23. Fig. 4 l appreciate the error bars on the ApRES derived $E_2 - E_1$. Please state more clearly how those were derived.

AC2.23. We state our error calculation in L206-207: "...with the associated phase error (standard deviation) estimated through the Cramer-Rao bound, following the methods of Jordan et al. (2019)". $E_2 - E_1$ is obtained directly through $d\Phi_{hhvv}/dz$, and the error is then transferred accordingly. We have made this clear with the addition of the following sentence (L218-219): "From here, estimates of $d\Phi_{hhvv}/dz$ and their respective errors for each depth bin were both scaled using Equation 7a to then produce estimates and uncertainties for $E_2 - E_1$."

RC2.24. l 289 This is not the "best model" that matches observed results. It is a model that explains some of the features in the observations

AC2.24. We have reworded this sentence to (L331-332): "The power anomaly model that we used to emulate measured results (Fig. 5a) incorporated a variable anisotropic scattering ratio…"

RC2.25. l 330 How fast does the ice-fabric structure adapt to a new strain regime? I think some sort of statement in this regard is required to better justify statements of ice-divide stability.

AC2.25. Brisbourne et al. (2019) states that, although the time taken to overprint a preexisting fabric is dependent on temperature, strain rate, and stress regime, it is poorly constrained excluding those from laboratory results. Therefore, we can implement the same reasoning as that of Brisbourne et al. (2019) and state that the measured COF distribution aligned with the observed surface strain orientation through depth reflects the current ice flow regime, assuming that the vertical assumption (i.e. E_2 - E_1) holds through the range of measured depths.

We have summarised the above explanation into Section 5.2 (L376-382):

> “Although the time taken to overprint a pre-existing fabric is poorly constrained, excluding those from laboratory results (Brisbourne et al. 2019), the removal of previous fabric evidence is thought to take significant time and may require anomalously strong deformation regimes (Alley 1988). At all sites, the alignment of our identified E_1 eigenvector orientation with the observed present-day strain regime is consistent with theory relating ice flow and crystal anisotropy (Azuma 1994). We are confident that the observed surface strain orientation likely reflects the current deformation regime, given this alignment, the temporal permanence of fabric signatures, and the comparatively short depth-age of our record.”

References

Brennan, P. V., Nicholls, K. W., Lok, L. B., and Corr, H. F. J.: Phase-sensitive FMCW radar system for high-precision Antarctic ice shelf profile monitoring, IET Radar, Sonar & Navigation, 8, 776–786, https://doi.org/10.1049/iet-rsn.2013.0053, 2014.

Brisbourne, A. M., Martín, C., Smith, A. M., Baird, A. F., Kendall, J. M., and Kingslake, J.: Constraining Recent Ice Flow History at Korff Ice Rise, West Antarctica, Using Radar and Seismic Measurements of Ice Fabric, Journal of Geophysical Research: Earth Surface, 124, 175–194, https://doi.org/10.1029/2018JF004776, 2019.

Burr, A., Noël, W., Trecourt, P., Bourcier, M., Gillet-Chaulet, F., Philip, A., and Martin, C. L.: The anisotropic contact response of viscoplastic monocrystalline ice particles, Acta Materialia, 132, 576–585, https://doi.org/10.1016/j.actamat.2017.04.069, 2017.

Dall, J.: Ice sheet anisotropy measured with polarimetric ice sounding radar, in: 30th International Geoscience and Remote Sensing Sympo- sium (IGARSS 2010), pp. 2507–2510, Honolulu, HI, https://doi.org/10.1109/IGARSS.2010.5653528, 2010.

Fujita, S., Maeno, H., and Matsuoka, K.: Radio-wave depolarization and scattering within ice sheets: A matrix-based model to link radar and ice-core measurements and its application, Journal of Glaciology, 52, 407–424, https://doi.org/10.3189/172756506781828548, 2006.

Horgan, H. J., Anandakrishnan, S., Alley, R. B., Burkett, P. G., and Peters, L. E.: Englacial seismic reflectivity: Imaging crystal-orientation fabric in West Antarctica, Journal of Glaciology, 57, 639–650, https://doi.org/10.3189/002214311797409686, 2011.

Howat, I. M., Porter, C., Smith, B. E., Noh, M.-J., and Morin, P.: The Reference Elevation Model of Antarctica, The Cryosphere, 13, 665–674, https://doi.org/10.5194/tc-2018-240, 2019.

Jordan, T. M., Schroeder, D. M., Castelletti, D., Li, J., and Dall, J.: A Polarimetric Coherence Method to Determine Ice Crystal Orientation Fabric From Radar Sounding: Application to the NEEM Ice Core Region, IEEE Transactions on Geoscience and Remote Sensing, pp. 1–17, https://doi.org/10.1109/tgrs.2019.2921980, 2019.

Jordan, T. M., Schroeder, D. M., Elsworth, C.W., and Siegfried, M. R.: Estimation of ice fabric within Whillans Ice Stream using polarimetric phase-sensitive radar sounding, Annals of Glaciology, 61, 74–83, https://doi.org/10.1017/aog.2020.6, 2020a.

Jordan, T. M., Martin, C., Brisbourne, A. C., Schroeder, D. M., and Smith, A. M.: Radar characterization of ice crystal orientation fabric and anisotropic rheology within an Antarctic ice stream, Earth and Space Science Open Archive ESSOAr, pp.1-48, https://doi.org/10.1002/essoar.10504765.1, 2020b.

Kennedy, J. H., Pettit, E. C., and Di Prinzio, C. L.: The evolution of crystal fabric in ice sheets and its link to climate history, Journal of Glaciology, 59, 357–373, https://doi.org/10.3189/2013JoG12J159, 2013.

Looyenga, H.: Dielectric constants of heterogeneous mixtures. Physica, 31, 401–406, https://doi.org/10.1016/0031-8914(65)90045-5, 1965.

Matsuoka, K., Power, D., Fujita, S., and Raymond, C. F.: Rapid development of anisotropic ice-crystal-alignment fabrics in- ferred from englacial radar polarimetry, central West Antarctica, Journal of Geophysical Research: Earth Surface, 117, 1–16, https://doi.org/10.1029/2012JF002440, 2012.

Morlighem, M., Rignot, E., Binder, T., Blankenship, D., Drews, R., Eagles, G., Eisen, O., Ferraccioli, F., Forsberg, R., Fretwell, P., Goel, V., Greenbaum, J. S., Gudmundsson, H., Guo, J., Helm, V., Hofstede, C., Howat, I., Humbert, A., Jokat, W., Karlsson, N. B., Lee, W. S., Matsuoka, K., Millan, R., Mouginot, J., Paden, J., Pattyn, F., Roberts, J., Rosier, S., Ruppel, A., Seroussi, H., Smith, E. C., Steinhage, D., Sun, B., van den Broeke, M. R., van Ommen, T. D., van Wessem, M., and Young, D. A.: Deep glacial troughs and stabilizing ridges unveiled beneath the margins of the Antarctic ice sheet, Nature Geoscience, 13, 132–137, https://doi.org/10.1038/s41561-019-0510-8, 2020.

Young, T. J., Schroeder, D. M., Christoffersen, P., Lok, L. B., Nicholls, K. W., Brennan, P. V., Doyle, S. H., Hubbard, B., and Hubbard, A.: Resolving the internal and basal geometry of ice masses using imaging phase-sensitive radar, Journal of Glaciology, 64, 649–660, https://doi.org/10.1017/jog.2018.54, 2018.